Individual Pitch Control

Inventory

T.G. van Engelen, E.L. van der Hooft

Abstract

The loads on the rotor blades, drive-train and tower of horizontal axis wind turbines are caused for a significant part by the rotational sampling of turbulence, the tower shadow and the windshear. These loads depend on the azimutal blade position and are approximately periodic in (multiples of) the rotational speed. It seems attractive to just add pure azimut dependent variations to the pitch angle of the individual blades. However, a small phase mismatch with respect to the tower shadow and windshear effect will cause higher instead of lower loads. Besides, the stochastic loads from the rotationally sampled turbulence are not reduced at all.

This inventory study concerns the design and potential of individual *feedback* pitch control for 3 bladed wind turbines. In this approach the danger of mismatch is avoided and the stochastic blade loads are also reduced. A simple design model is derived for the parametrisation of the feedback loops for individual pitch control around one time the rotational frequency (1p). Rainflow counts and power spectra obtained from time-domain simulations give an indication of the achievable reduction of loads. In addition, the concept of individual pitch control is extendend to multiples of the rotational frequency (2p, 3p; multi-mode pitch control). Scoping calculations show a significant further reduction of blade loads as well as a reduction of 3p harmonics in tilt and yaw loads in the nacelle.

Acknowledgement

Pieter Schaak (ECN) is acknowledged for fruitful technical discussions and project coordination.
Jaap ’t Hooft (Novem) is acknowledged for project steering.

CONTENTS

1 INTRODUCTION

This study concerns the design and potential of individual *feedback* pitch control for 3 bladed wind turbines. It belongs to the project 'Ontwerpgereedschap voor het integraal ontwerpen van windturbineregelingen', funded by Novem under grant 2020-01-12-10-003 (ECN project number 7.4153).

The loads on the rotor blades, drive-train and tower of horizontal axis wind turbines are caused for a significant part by the rotational sampling of turbulence, the tower shadow and the windshear. These loads can be reduced via individual pitch control. Earlier publications [1], [2] give an impression of the potential of this control concept, focussed on load reduction around one time the rotational frequency (1p). However a simple design method for *feedback based* individual pitch control has not yet been published.

In order to avoid these feedback loops, which may be sensitive to instability, it seems attractive to just add pure azimut dependent variations to the pitch angle of the individual blades. However, a small phase mismatch with respect to the tower shadow and windshear effect will cause higher instead of lower loads. Besides, the stochastic loads from the rotationally sampled turbulence are then not reduced at all.

The approach described in this report yields a simple design model for the parametrisation of *feedback loops* for individual pitch control. It enables the industrially accepted stability assessment method by Bode (phase and gain margin). Thus the danger of 'azimutal mismatch' is avoided, turbulence induced loads are reduced as well, and the senstivity to instability can be well quantified via the phase and gain margins of the control loops.

The following topics are addressed in this report

- mapping a standard model to a design model for individual pitch control;
- design of feedback loops for collective pitch and individual pitch control;
- time-domain simulation and assessment of loads on blades and nacelle.

2 MODEL FOR INDIVIDUAL PITCH CONTROL

A design model for individual pitch control is derived for 3 bladed rotors by a multi-blade coordinate transformation on the pitch command signals and on the flap- and leadwise blade root moments (blade-associated model inputs and outputs).

The point of departure for the control design model comprises the first bending mode of the tower in nodding and naying direction, characterised by hub height H, tower top effective mass M, linear stiffness S and damping constant D, and the overall inertia J of the drive-train and rotor:

$$\begin{aligned} J \cdot \tfrac{\mathrm{d}}{\mathrm{dt}}(\Omega) &= M_{\mathrm{rotor}} \\ M \cdot \tfrac{\mathrm{d}^2}{\mathrm{dt}^2}(s_{\mathrm{nod}}) + D \cdot \tfrac{\mathrm{d}}{\mathrm{dt}}(s_{\mathrm{nod}}) + S \cdot s_{\mathrm{nod}} &= F_{\mathrm{ax}} - \tfrac{3/2}{H} \cdot M_{\mathrm{tilt}} \\ M \cdot \tfrac{\mathrm{d}^2}{\mathrm{dt}^2}(s_{\mathrm{nay}}) + D \cdot \tfrac{\mathrm{d}}{\mathrm{dt}}(s_{\mathrm{nay}}) + S \cdot s_{\mathrm{nay}} &= F_{\mathrm{sd}} + \tfrac{3/2}{H} \cdot M_{\mathrm{rotor}} \end{aligned} \tag{2.1}$$

with shaft moment M_{rotor}, axial force F_{ax}, tilt moment M_{tilt} and sideward force $F_{\mathrm{sd}}$by:

$$\begin{aligned} M_{\mathrm{rotor}} &= k_{\mathrm{M_x}} \cdot (\theta_1 + \theta_2 + \theta_3) + h_{\mathrm{M_x}} \cdot (u_1 + u_2 + u_3) - 3 \cdot h_{\mathrm{M_x}} \cdot \tfrac{\mathrm{d}}{\mathrm{dt}}(s_{\mathrm{nod}}) \\ F_{\mathrm{ax}} &= k_{\mathrm{F_x}} \cdot (\theta_1 + \theta_2 + \theta_3) + h_{\mathrm{F_x}} \cdot (u_1 + u_2 + u_3) - 3 \cdot h_{\mathrm{F_x}} \cdot \tfrac{\mathrm{d}}{\mathrm{dt}}(s_{\mathrm{nod}}) \\ M_{\mathrm{tilt}} &= \sum_{i=1}^{3} \left[\sin\psi_i \cdot (-k_{\mathrm{M_z}} \cdot \theta_i - h_{\mathrm{M_x}} \cdot u_i + h_{\mathrm{M_x}} \cdot \tfrac{\mathrm{d}}{\mathrm{dt}}(s_{\mathrm{nod}})) \right] \\ F_{\mathrm{sd}} &= \sum_{i=1}^{3} \left[\sin\psi_i \cdot (-k_{\mathrm{F_z}} \cdot \theta_i - h_{\mathrm{F_z}} \cdot u_i + h_{\mathrm{F_z}} \cdot \tfrac{\mathrm{d}}{\mathrm{dt}}(s_{\mathrm{nod}})) \right] \end{aligned} \tag{2.2}$$

The model input variables $\{\theta_i | i = 1,2,3\}$ and $\{u_i | i = 1,2,3\}$ are the blade specific pitch angle variations and the blade effective wind speed variations. The variables $\{\psi_i | i = 1,2,3\}$ are the azimut angles of the rotor blades, given by:

$$\begin{aligned} \psi_1(t) &= \textstyle\int_{-\infty}^{t} \Omega(\tau)\mathrm{d}\tau \\ \psi_2(t) &= \psi_1(t) + \tfrac{2}{3}\pi \\ \psi_3(t) &= \psi_2(t) + \tfrac{2}{3}\pi \end{aligned} \tag{2.3}$$

The *angular* nodding speed $\frac{\mathrm{d}}{\mathrm{dt}}(\phi_{\mathrm{nod}})$, which equals about $\frac{3/2}{H} \cdot \frac{\mathrm{d}}{\mathrm{dt}}(s_{\mathrm{nod}})$, is neglected in the control design model. It augments the relative axial wind speed on the i^{th} rotor blade with approximately $3/4 \cdot R_{\mathrm{b}} \cdot \sin(\psi_i) \cdot \frac{\mathrm{d}}{\mathrm{dt}}(\phi_{\mathrm{nod}})$. This feature *has been* taken into account in the simulation of the wind turbine behaviour in chapter 4 on the assessment of individual pitch control.

The used gains from pitch and wind speed variations (k..., h...) towards aerodynamic loads per blade in the rotor centre have the following meaning (all derived from power and thrust coefficient data; see A):

$$\begin{aligned} k_{\mathrm{M_x}}, h_{\mathrm{M_x}} &: \text{gains related to leadwise moment} \\ k_{\mathrm{F_x}}, h_{\mathrm{F_x}} &: \text{gains related to flapwise force} \\ k_{\mathrm{M_z}}, h_{\mathrm{M_x}} &: \text{gains related to flapwise moment} \\ k_{\mathrm{F_z}}, h_{\mathrm{F_z}} &: \text{gains related to leadwise force} \end{aligned} \tag{2.4}$$

This 'standard control design model formulation' can be written as a first order vector state space representation in which the output vector equation comprises the variables to be controlled, viz. the rotor speed Ω and the flapwise blade root moments $\{M_{z_i}|i=1,2,3\}$

$$\begin{aligned} \tfrac{\mathrm{d}}{\mathrm{dt}}(\underline{z}) &= A\cdot\underline{z}+B\cdot\underline{v} \quad ; \quad \underline{z} = |s_{\mathrm{nod}}\ \ s_{\mathrm{nay}}\ \ \Omega\ \ v_{\mathrm{nod}}\ \ v_{\mathrm{nay}}|'; \\ & \qquad\qquad\qquad\quad \underline{v} = |u_1\ \ u_2\ \ u_3\ \ \theta_1\ \ \theta_2\ \ \theta_3|' \\ \underline{y} &= C\cdot\underline{z}+K\cdot\underline{v} \quad ; \quad \underline{y} = |\Omega\ \ M_{z_1}\ \ M_{z_2}\ \ M_{z_3}|' \end{aligned} \tag{2.5}$$

The contributing scalar state transition equations are:

$$\begin{aligned} \tfrac{\mathrm{d}}{\mathrm{dt}}(s_{\mathrm{nod}}) &= v_{\mathrm{nod}} \\ \tfrac{\mathrm{d}}{\mathrm{dt}}(s_{\mathrm{nay}}) &= v_{\mathrm{nay}} \\ \tfrac{\mathrm{d}}{\mathrm{dt}}(\Omega) &= \tfrac{1}{J}\cdot\Big[\sum_{i=1}^{3}\big[k_{\mathrm{M_x}}\cdot\theta_i\big]+\sum_{i=1}^{3}\big[h_{\mathrm{M_x}}\cdot(u_i-v_{\mathrm{nod}})\big]\Big] \\ \tfrac{\mathrm{d}}{\mathrm{dt}}(v_{\mathrm{nod}}) &= \tfrac{1}{M}\cdot\Big[-D\cdot v_{\mathrm{nod}}-S\cdot s_{\mathrm{nod}}+\sum_{i=1}^{3}\big[k_{\mathrm{F_x}}\cdot\theta_i+h_{\mathrm{F_x}}\cdot(u_i-v_{\mathrm{nod}})\big] \\ &\quad -\tfrac{3/2}{H}\cdot\sum_{i=1}^{3}\big[\sin\psi_i\cdot(k_{\mathrm{M_z}}\cdot\theta_i+h_{\mathrm{M_x}}\cdot(u_i-v_{\mathrm{nod}}))\big]\Big] \\ \tfrac{\mathrm{d}}{\mathrm{dt}}(v_{\mathrm{nay}}) &= \tfrac{1}{M}\cdot\Big[-D\cdot v_{\mathrm{nay}}-S\cdot s_{\mathrm{nay}}+\tfrac{3/2}{H}\cdot\sum_{i=1}^{3}\big[k_{\mathrm{M_x}}\cdot\theta_i+h_{\mathrm{M_x}}\cdot(u_i-v_{\mathrm{nod}})\big] \\ &\quad -\sum_{i=1}^{3}\big[\sin\psi_i\cdot(k_{\mathrm{F_z}}\cdot\theta_i+h_{\mathrm{F_z}}\cdot(u_i-v_{\mathrm{nod}}))\big]\Big] \end{aligned} \tag{2.6}$$

and the scalar output equations are:

$$\begin{aligned} \Omega &= 1\cdot\Omega \\ M_{z_i} &= k_{\mathrm{M_z}}\cdot\theta_i+h_{\mathrm{M_x}}\cdot(u_i-v_{\mathrm{nod}}) \qquad i=1,2,3 \end{aligned} \tag{2.7}$$

Figure 2.1 gives a comprehensive view on the wind turbine model by eq. 2.6 and 2.7 with periodic coefficients.

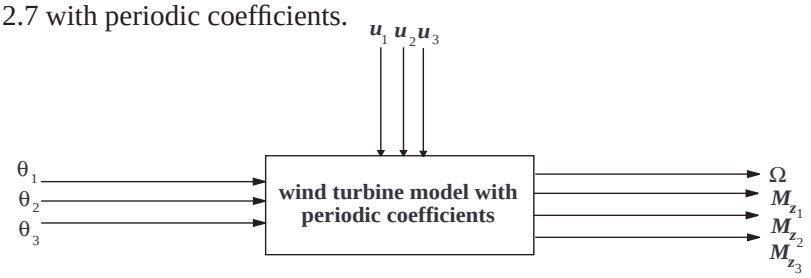

Figure 2.1: Visualisation of wind turbine model by eq. 2.6 and 2.7

The state transition and output equations are reordered such that the variables in the right hand side arise from left to right as 'state variables', 'control inputs'

(pitch angle variations) and 'disturbance inputs' (blade effective wind speed variatons):

$$\begin{aligned}
\tfrac{\mathrm{d}}{\mathrm{dt}}(s_{\mathrm{nod}}) &= v_{\mathrm{nod}} \\
\tfrac{\mathrm{d}}{\mathrm{dt}}(s_{\mathrm{nay}}) &= v_{\mathrm{nay}} \\
\tfrac{\mathrm{d}}{\mathrm{dt}}(\Omega) &= \tfrac{1}{J}\cdot\big[-3\cdot h_{\mathrm{M_x}}\cdot v_{\mathrm{nod}} + k_{\mathrm{M_x}}\cdot\sum_{i=1}^{3}\big[\theta_i\big] + h_{\mathrm{M_x}}\cdot\sum_{i=1}^{3}\big[u_i\big]\big] \\
\tfrac{\mathrm{d}}{\mathrm{dt}}(v_{\mathrm{nod}}) &= \tfrac{1}{M}\cdot\big[-(D+3\cdot h_{\mathrm{F_x}} - \tfrac{3/2}{H}\cdot h_{\mathrm{M_x}}\cdot\sum_{i=1}^{3}\big[\sin\psi_i\big])\cdot v_{\mathrm{nod}} - S\cdot s_{\mathrm{nod}} + \\
&\quad \sum_{i=1}^{3}\big[(k_{\mathrm{F_x}} - \tfrac{3/2}{H}\cdot k_{\mathrm{M_z}}\cdot\sin\psi_i)\cdot\theta_i\big] + \sum_{i=1}^{3}\big[(h_{\mathrm{F_x}} - \tfrac{3/2}{H}\cdot h_{\mathrm{M_x}}\cdot\sin\psi_i)\cdot u_i\big]\big] \\
\tfrac{\mathrm{d}}{\mathrm{dt}}(v_{\mathrm{nay}}) &= \tfrac{1}{M}\cdot\big[-D\cdot v_{\mathrm{nay}} - S\cdot s_{\mathrm{nay}} + \sum_{i=1}^{3}\big[-\tfrac{3/2}{H}\cdot h_{\mathrm{M_x}} + h_{\mathrm{F_z}}\cdot\sin\psi_i\big]\cdot v_{\mathrm{nod}} \\
&\quad \sum_{i=1}^{3}\big[(\tfrac{3/2}{H}\cdot k_{\mathrm{M_x}} - \sin\psi_i\cdot k_{\mathrm{F_z}})\cdot\theta_i\big] + \sum_{i=1}^{3}\big[(\tfrac{3/2}{H}\cdot h_{\mathrm{M_x}} - \sin\psi_i\cdot h_{\mathrm{F_z}})\cdot u_i\big]\big]
\end{aligned} \tag{2.8}$$

and:

$$\begin{aligned}
\Omega &= 1\cdot\Omega \\
M_{z_i} &= k_{\mathrm{M_z}}\cdot\theta_i + h_{\mathrm{M_x}}\cdot(u_i - v_{\mathrm{nod}}) \qquad i = 1,2,3
\end{aligned} \tag{2.9}$$

We decided to use a multi-blade coordinate transformation as proposed by Coleman and Feingold [3] for the model inputs and outputs that are attached to the blades. This yields 'blade variables' in the 'fixed coordinate system'. Since the design model does not contain *non-coaxial* state variables attached to the rotating shaft or rotor blades, a similar state variable transformation does not apply. The following mappings hold between the real blade variables and their transformations in the 'fixed coordinate system' (superscript '^{cm}'):

$$\begin{aligned}
\begin{bmatrix}\theta_1\\ \theta_2\\ \theta_3\end{bmatrix} &= \begin{pmatrix}1 & \sin\psi_1 & \cos\psi_1\\ 1 & \sin\psi_2 & \cos\psi_2\\ 1 & \sin\psi_3 & \cos\psi_3\end{pmatrix}\cdot\begin{bmatrix}\theta_1^{\mathrm{cm}}\\ \theta_2^{\mathrm{cm}}\\ \theta_3^{\mathrm{cm}}\end{bmatrix} \\
\begin{bmatrix}M_{z_1}^{\mathrm{cm}}\\ M_{z_2}^{\mathrm{cm}}\\ M_{z_3}^{\mathrm{cm}}\end{bmatrix} &= \begin{pmatrix}\frac{1}{3} & \frac{1}{3} & \frac{1}{3}\\ \frac{2}{3}\sin\psi_1 & \frac{2}{3}\sin\psi_2 & \frac{2}{3}\sin\psi_3\\ \frac{2}{3}\cos\psi_1 & \frac{2}{3}\cos\psi_2 & \frac{2}{3}\cos\psi_3\end{pmatrix}\begin{bmatrix}M_{z_1}\\ M_{z_2}\\ M_{z_3}\end{bmatrix}
\end{aligned} \tag{2.10}$$

The upper matrix above also maps u_i^{cm} to u_i.

The meaning of the Coleman-transformed model inputs, that is to say the multi-blade coordinates of the pitch and wind speed vector 'in the fixed coordinate system', is as follows:

$$\begin{aligned}
\theta_1^{\mathrm{cm}},\ u_1^{\mathrm{cm}} &: \text{inputs related to axial force and rotor moment} \\
\theta_2^{\mathrm{cm}},\ u_2^{\mathrm{cm}} &: \text{inputs related to tiltwise moment} \\
\theta_3^{\mathrm{cm}},\ u_3^{\mathrm{cm}} &: \text{inputs related to yawwise moment}
\end{aligned} \tag{2.11}$$

The second and third multi-blade coordinate of the flapwise blade root moment ($M_{z_2}^{\mathrm{cm}}$, $M_{z_3}^{\mathrm{cm}}$) are related to the tilt and yaw moment in the rotor centre. In the same way the corresponding multi-blade coordinates of the pitchwise blade root moment would be related to the yaw and tilt moment respectively. Since we neglect the pitchwise blade root moments it holds:

$$\begin{aligned} M_{z_2}^{\mathrm{cm}} &= -\tfrac{2}{3} \cdot M_{\mathrm{tilt}} \quad \text{(in rotor centre; } M_{\mathrm{tilt}} < 0\text{: tilt upward)} \\ M_{z_3}^{\mathrm{cm}} &= \tfrac{2}{3} \cdot M_{\mathrm{yaw}} \quad \text{(in rotor centre; } M_{\mathrm{yaw}} > 0\text{: yaw clockwise at top-down view)} \end{aligned} \tag{2.12}$$

The first multi-blade coordinate, $M_{z_1}^{\mathrm{cm}}$, has not an interpretable physical meaning. For all multi-blade coordinates of the flapwise blade root moment, the expressions in multi-blade coordinates of the input variables are time-invariant.

We now substitute the input mappings from Eq. 2.10 in the re-arranged state space and output equations and in addition we replace the three flapwise blade root moment as output variables by the second and third corresponding multi-blade coordinates. This yields the pursued control design model with time-invariant state transition equations:

$$\begin{aligned} \tfrac{\mathrm{d}}{\mathrm{dt}}(s_{\mathrm{nod}}) &= v_{\mathrm{nod}} \\ \tfrac{\mathrm{d}}{\mathrm{dt}}(s_{\mathrm{nay}}) &= v_{\mathrm{nay}} \\ \tfrac{\mathrm{d}}{\mathrm{dt}}(\Omega) &= \tfrac{1}{J} \cdot \Big(-3 \cdot h_{\mathrm{M_x}} \cdot v_{\mathrm{nod}} + 3 \cdot k_{\mathrm{M_x}} \cdot \theta_1^{\mathrm{cm}} + 3 \cdot h_{\mathrm{M_x}} \cdot u_1^{\mathrm{cm}} \Big) \\ \tfrac{\mathrm{d}}{\mathrm{dt}}(v_{\mathrm{nod}}) &= \tfrac{1}{M} \cdot \Big(-(D + 3 \cdot h_{\mathrm{F_x}}) \cdot v_{\mathrm{nod}} - S \cdot s_{\mathrm{nod}} + 3 \cdot k_{\mathrm{F_x}} \cdot \theta_1^{\mathrm{cm}} + \tfrac{2.25}{H} \cdot k_{\mathrm{M_z}} \cdot \theta_2^{\mathrm{cm}} + \\ &\quad 3 \cdot h_{\mathrm{F_x}} \cdot u_1^{\mathrm{cm}} + \tfrac{2.25}{H} \cdot h_{\mathrm{M_x}} \cdot u_2^{\mathrm{cm}} \Big) \\ \tfrac{\mathrm{d}}{\mathrm{dt}}(v_{\mathrm{nay}}) &= \tfrac{1}{M} \cdot \Big(D \cdot v_{\mathrm{nay}} - S \cdot s_{\mathrm{nay}} + \tfrac{4.5}{H} \cdot h_{\mathrm{M_x}} \cdot v_{\mathrm{nod}} + \tfrac{4.5}{H} \cdot k_{\mathrm{M_x}} \cdot \theta_1^{\mathrm{cm}} - 1.5 \cdot k_{\mathrm{F_z}} \cdot \theta_2^{\mathrm{cm}} + \\ &\quad \tfrac{4.5}{H} \cdot h_{\mathrm{M_x}} \cdot u_1^{\mathrm{cm}} - 1.5 \cdot k_{\mathrm{F_z}} \cdot u_2^{\mathrm{cm}} \Big) \end{aligned} \tag{2.13}$$

and output equations:

$$\begin{aligned} \Omega &= 1 \cdot \Omega && \rightarrow \text{feedback to } \theta_1^{\mathrm{cm}} \text{ for rotor speed regulation} \\ M_{z_1}^{\mathrm{cm}} &= k_{\mathrm{M_z}} \cdot \theta_1^{\mathrm{cm}} + h_{\mathrm{M_z}} \cdot u_1^{\mathrm{cm}} - h_{\mathrm{M_z}} \cdot v_{\mathrm{nod}} && \rightarrow \text{no feedback} \\ M_{z_2}^{\mathrm{cm}} &= k_{\mathrm{M_z}} \cdot \theta_2^{\mathrm{cm}} + h_{\mathrm{M_z}} \cdot u_2^{\mathrm{cm}} && \rightarrow \text{feedback to } \theta_2^{\mathrm{cm}} \text{ for reduction 1p flap and 0p tilt loads} \\ M_{z_3}^{\mathrm{cm}} &= k_{\mathrm{M_z}} \cdot \theta_3^{\mathrm{cm}} + h_{\mathrm{M_z}} \cdot u_3^{\mathrm{cm}} && \rightarrow \text{feedback to } \theta_3^{\mathrm{cm}} \text{ for reduction 1p flap and 0p yaw loads} \end{aligned} \tag{2.14}$$

Figure 2.2 gives a comprehensive view on the wind turbine model by eq. 2.13 and 2.14 with time invariant coefficients. The matrices P and P^{-1} are equal to the respective matrices in eq. 2.10:

$$P = \begin{pmatrix} 1 & \sin\psi_1 & \cos\psi_1 \\ 1 & \sin\psi_2 & \cos\psi_2 \\ 1 & \sin\psi_3 & \cos\psi_3 \end{pmatrix} \quad ; \quad P^{-1} = \begin{pmatrix} \frac{1}{3} & \frac{1}{3} & \frac{1}{3} \\ \frac{2}{3}\sin\psi_1 & \frac{2}{3}\sin\psi_2 & \frac{2}{3}\sin\psi_3 \\ \frac{2}{3}\cos\psi_1 & \frac{2}{3}\cos\psi_2 & \frac{2}{3}\cos\psi_3 \end{pmatrix} \tag{2.15}$$

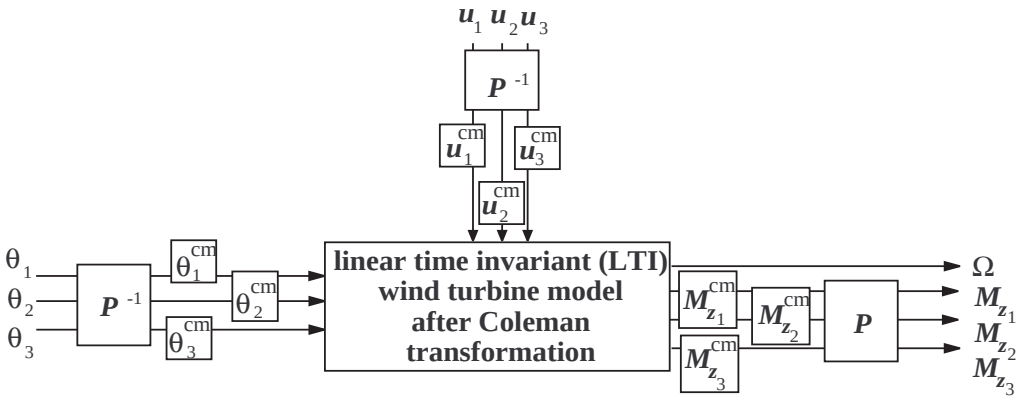

Figure 2.2: Visualisation of wind turbine model by eq. 2.13 and 2.14

3 SYNTHESIS OF INDIVIDUAL PITCH CONTROL

Feedback loops for collective pitch control and individual pitch control are fit on the three non-interacting transfer functions from the transformed pitch command signals to the rotor speed and the tilt- and yawwise transformation results (multi-blade coordinates) of the flapwise blade root moments. The concept of individual pitch control is extendend to multiples of the rotational frequency (2p, 3p; multi-rotational-mode pitch control).

The figures 3.1 up to 3.3 show that three scalar linear time invariant feedback loops can be used for rotor speed regulation and reduction of (1p) blade loads and (0p) tilt and yaw loads. These feedback loops act 'in between the inverse Coleman transformation P^{-1} of measurement signals and the Coleman transformation P on control signals'.

Figure 3.1 shows the layout of this controller configuration together with the wind turbine model with periodic coefficients, that is to say the 'real' feedback system. The feedback loops map the rotational speed and the 2$^{\mathrm{nd}}$ and 3$^{\mathrm{rd}}$ coordinate of the Coleman transformation of the flapwise blade root moments to the three pitch related inputs that set up the blade individual pitch angles after they have been subjected to the inverse Coleman transformation (remodulation).

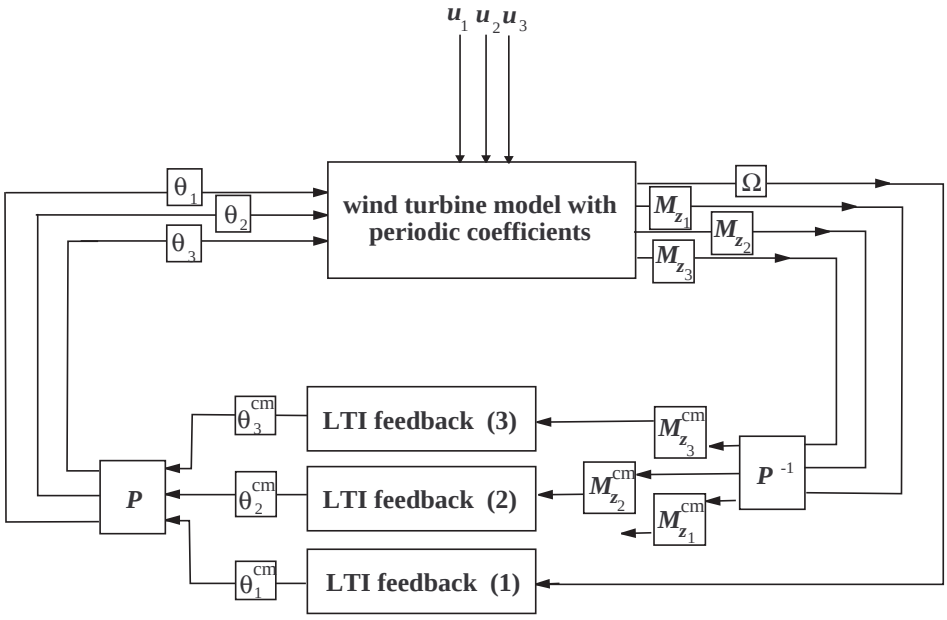

Figure 3.1: wind turbine model with periodic coefficients and three LTI-feedback loops between demodulated measurenent signals and control signals to be remodulated ('real feedback system')

Figures 3.2 and 3.3 clarify that the feedback of demodulated measurement signals and emission of remodulated control signals on the 'real turbine' is identical to pure linear time invariant feedback on the 'linear time invariant (LTI) transformed turbine model' in the 'control directions' of the rotor, tilt and yaw moment.

Figure 3.2 shows the 'real' feedback system extended with products of the Cole-

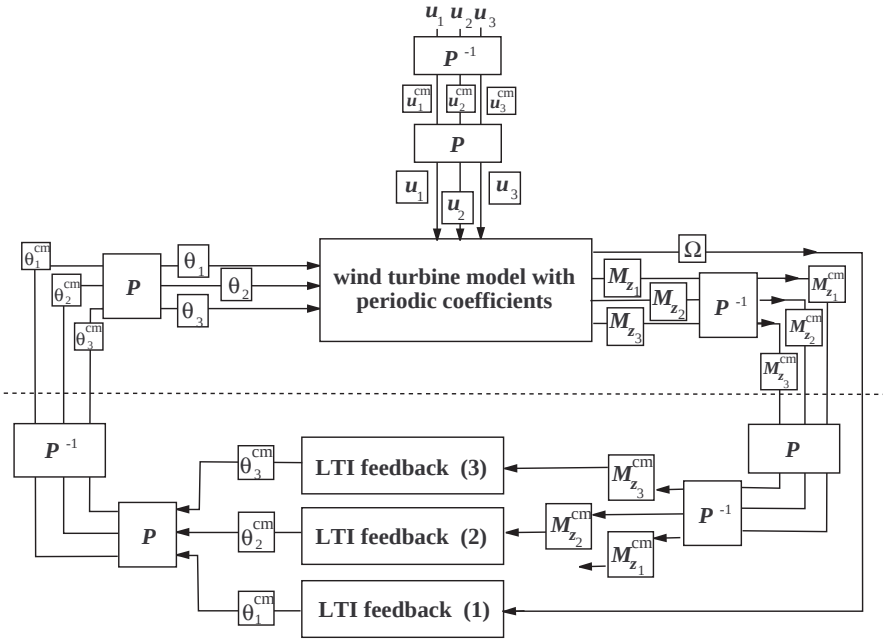

Figure 3.2: Feedback system extended with products of Colemant transformation matrix (P) and its inverse

man transformation matrix P and its inverse P^{-1}. If the 'wind turbine part' is seperated from the 'control part' in the feedback scheme *just between* the added matrix products $P \cdot P^{-1}$ and $P^{-1} \cdot P$ then a linear time invariant wind turbine and controller model arise. This wind turbine model is exactly the one described by eq. 2.13 and 2.14. This results in the LTI feedback scheme of figure 3.3. The LTI wind turbine model thus is the control design model for combined collective and individual pitch control

This control design model aslo appears to consist of *non-two-sided interacting* transfer functions can be derived for the rotor speed Ω and the tilt- and yawwise multi-blade coordinates $M_{z_2}^{\mathrm{cm}}$ and $M_{z_3}^{\mathrm{cm}}$ of the flapwise moments. Thus *linear time invariant* **scalar** *contol synthesis* is allowed. The transfer functions follow from the state space model by eq. 2.13 and 2.14 in which the time-derivative operator $\frac{\mathrm{d}}{\mathrm{dt}}$ is replaced by the Laplace operator s, which can be considered as the frequency multiplier in the transfer function formulations. In addition, an overall control delay of τ_{v} seconds is added to the transfer functions with the multi-blade pitch

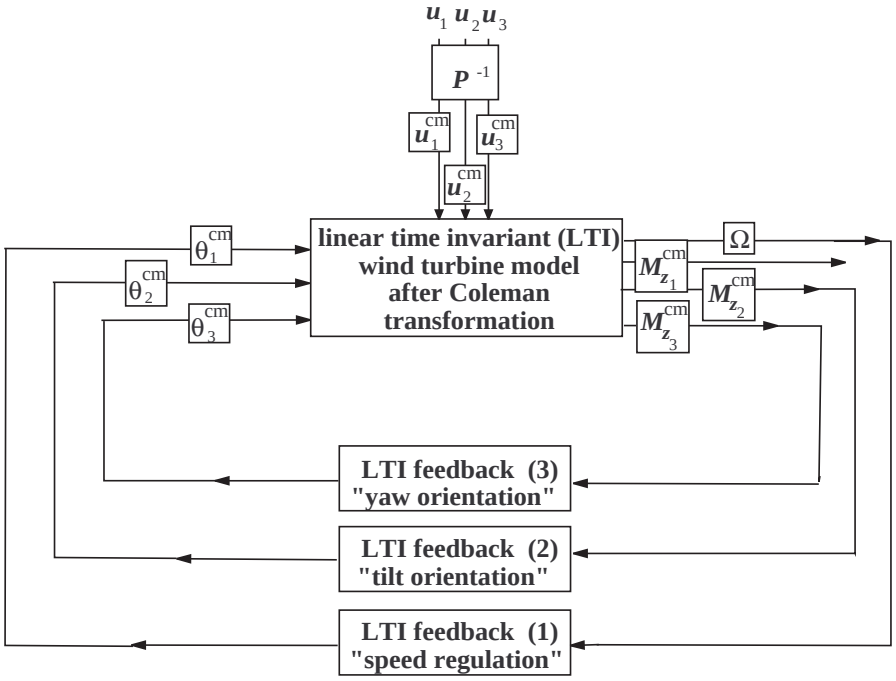

Figure 3.3: LTI-transformed wind turbine model model with three LTI feedback loops (control design feedback system

angle coordinates as input by inclusion of the factor $\mathrm{e}^{-\tau_\mathrm{v}\cdot\mathrm{s}}$:

$$
\begin{aligned}
\Omega \quad &= \quad \frac{1}{J\cdot\mathrm{s}}\cdot\Big(3k_{\mathrm{M_x}} - \frac{9h_{\mathrm{M_x}}\cdot k_{\mathrm{F_x}}\cdot\mathrm{s}}{M\cdot\mathrm{s}^2+(D+3k_{\mathrm{F_x}})\cdot\mathrm{s}+S}\Big)\cdot\mathrm{e}^{-\tau_\mathrm{v}\cdot\mathrm{s}}\cdot\theta_1^{\mathrm{cm}}+ \\
&\quad\ \frac{1}{J\cdot\mathrm{s}}\cdot\Big(-\frac{3h_{\mathrm{M_x}}\cdot\frac{2.25}{H}k_{\mathrm{M_z}}\cdot\mathrm{s}}{M\cdot\mathrm{s}^2+(D+3k_{\mathrm{F_x}})\cdot\mathrm{s}+S}\Big)\cdot\mathrm{e}^{-\tau_\mathrm{v}\cdot\mathrm{s}}\cdot\theta_2^{\mathrm{cm}}+ \\
&\quad\ \frac{1}{J\cdot\mathrm{s}}\cdot\Big(3h_{\mathrm{M_x}} - \frac{9h_{\mathrm{M_x}}\cdot h_{\mathrm{F_x}}\cdot\mathrm{s}}{M\cdot\mathrm{s}^2+(D+3k_{\mathrm{F_x}})\cdot\mathrm{s}+S}\Big)\cdot u_1^{\mathrm{cm}}+ \\
&\quad\ \frac{1}{J\cdot\mathrm{s}}\cdot\Big(-\frac{3h_{\mathrm{M_x}}\cdot\frac{2.25}{H}h_{\mathrm{M_z}}\cdot\mathrm{s}}{M\cdot\mathrm{s}^2+(D+3k_{\mathrm{F_x}})\cdot\mathrm{s}+S}\Big)\cdot\cdot u_2^{\mathrm{cm}} \\
M_{z_2}^{\mathrm{cm}} \quad &= \quad k_{\mathrm{M_z}}\cdot\mathrm{e}^{-\tau_\mathrm{v}\cdot\mathrm{s}}\cdot\theta_2^{\mathrm{cm}} + h_{\mathrm{M_z}}\cdot u_2^{\mathrm{cm}} \\
M_{z_3}^{\mathrm{cm}} \quad &= \quad k_{\mathrm{M_z}}\cdot\mathrm{e}^{-\tau_\mathrm{v}\cdot\mathrm{s}}\cdot\theta_3^{\mathrm{cm}} + h_{\mathrm{M_z}}\cdot u_3^{\mathrm{cm}}
\end{aligned}
\tag{3.1}
$$

These transfer functions show that in addition to $M_{z_2}^{\mathrm{cm}}$ the input θ_2^{cm} affects the output Ω, but there is no coupling between Ω and $M_{z_2}^{\mathrm{cm}}$. The transfer function coupling is thus *one-sided*, so there is no interaction. This allows to consider independent control loops for all three transfer functions; the control loop from $M_{z_2}^{\mathrm{cm}}$ to θ_2^{cm} will yield an independent 'disturbance signal' on the control loop for Ω. Since the tower bending dynamics only play a role in frequencies far above the frequency bandwidth for the rotor speed regulation, it satisfies to use the following

three ‘process transfer functions’ for control synthesis.

$$\begin{aligned} \Omega &= \frac{1}{J \cdot \mathrm{s}} \cdot \left(3 k_{\mathrm{M_x}}\right) \cdot \mathrm{e}^{-\tau_{\mathrm{v}} \cdot \mathrm{s}} \cdot \theta_1^{\mathrm{cm}} \\ M_{z_2}^{\mathrm{cm}} &= k_{\mathrm{M_z}} \cdot \mathrm{e}^{-\tau_{\mathrm{v}} \cdot \mathrm{s}} \cdot \theta_2^{\mathrm{cm}} \\ M_{z_3}^{\mathrm{cm}} &= k_{\mathrm{M_z}} \cdot \mathrm{e}^{-\tau_{\mathrm{v}} \cdot \mathrm{s}} \cdot \theta_3^{\mathrm{cm}} \end{aligned} \tag{3.2}$$

Stability analysis afterwards *does* include the tower dynamics in the rotor speed control loop, in order to be sure that no instability occurs beyond the control bandwidth for Ω.

The speed regulation loop consists of PI-feedback of the measured rotor speed Ω to the desired pitch angle θ_1^{cm}, extended with a low pass filter with 14db reduction or more for fluctuations above $2.5 \cdot f_0$ Hz (f_0 is the rotational frequency).

The ‘1p load reduction loops’ consist of I-feedback from the second and third multi-blade flap moment coordinate ($M_{z_2}^{\mathrm{cm}}$, $M_{z_3}^{\mathrm{cm}}$) to the second and third multi-blade pitch angle (θ_1^{cm}, θ_2^{cm}), extended with a band pass filter for 3p signal components and a low pass filter for 6p fluctations and higher. The filters are active *after* de modulation of the blade flap moment measurements.

The parametrisation of the three feedback loops has been based on stability assessment according to Bode (phase and gain margin). Three completely independent feedback loops were assumed with an overall loop delay of 0.2 s included, which caters for the dynamics of control data processing and pitch actuation.

Multi-rotational-mode reduction loops
In addition ‘2p and 3p load reduction loops’ have been designed. The layout of these loops is nearly the same as the ‘1p load reduction loops’. However, the de modulation of flapwise root moment signals and remodulation of yaw- and pitch oriented pitch signals occurs with transformation matrices that are periodic in 2Ω and 3Ω respectively. These loops also include 3p band pass and 6p low pass filters, which are effective *after* 2p, respectively 3p, demodulation of the flap moment measurements.

It has been assumed that because of the use of the filters after modulation, it is allowed to apply ‘parallel operating feedback loops’ that actually effectuate 1p, 2p and 3p pitch actions. Design *simulations* showed sufficient stability margins in the sense of allowed magnification of loop gains and overall control delay. However *analytic stability* assessment for this *multi-rotational-mode* control is still required. This requires application of Floquet theory, because the ‘design feedback scheme’ now will have periodic coefficients that cannot be eliminated.

4 SIMULATION AND LOAD ASSESSMENT

Simulations in the time-domain are performed with correlated blade effective wind speed signals, which incorporate turbulence as well as tower shadow and wind shear. Four cases are addressed:

- collective pitch control only;
- collective pitch control as well as 1p individual pitch control;
- collective pitch control as well as 1p and 2p individual pitch control;
- collective pitch control as well as 1p, 2p and 3p individual pitch control.

Autopower spectra and load histograms of the blade root flap moment and the tilt and yaw moment on the nacelle were derived from six realisations of 800 seconds each in all cases. The simulation was set up by the below listed main features of the wind turbine, wind data and opetational data. The controller settings as discussed in the previous chapter did apply. Both the control and wind turbine have been simulated with linear differential equations while the calculated azimut angle had been used for the position dependent blade behaviour. Blade effective wind speed signals had been generated as an extension to the commonly used rotor effective wind speed signal. The blade effective wind speed is obtained by integrating the space dependent turbulence, as well as the tower stagnation and wind shear effects, over the radius of the rotating rotor blade. The coherence of the wind speed between the blades has been taken into account completely .

Main features wind turbine
rotor diameter: 90m
number of blades: 3
overall control dynamics: delay of 0.2s
rotor inertia: $12 \cdot 10^6$ kgm^2
tower height: 70 m
top equivalent overal tower mass : $265 \cdot 10^3$ kg
natural frequency tower + rotor + nacelle: 0.35 Hz
average tower diameter for tower stagnation: 2.5 m
average distance from blade to tower for tower stagnation: 5.0 m

Wind data
shear coefficient: 0.12
turbulence intensity at 15 m/s: 16%
ESDU auto power spectrum
Kaimal coherence function
air density: 1.225 kg/m^3

Operational data
average wind speed : 15 m/s
average rotor speed: 15 rpm
average pitch angle: 10 degr

Simulation results

Figures 4.1 and 4.2 show realisations of the flapwise blade root moment and the tilt moment on the nacelle in the rotor centre. Figure 4.3 shows the corresponding pitch angles of one blade for the different control options. Each graph shows the 0p control actions. The upper graph shows the overall pitch signals that also suppress the 1st mode of the sampled wind speed for the three blades (120 dg phase shift). The middle graph show the additional pitch actions when also the 2nd mode of the sampled windspeed is suppressed (240 dg phase shift). The lower graph shows the additional effort for the 3rd mode (360 dg phase shift). Though the additional pitch angle excursions in the 2p and 3p rotational modes are moderate, the belonging pitch speeds are considerable, especially for the 3p-mode suppression. The belonging pitch speeds and accelerations are visualised in figures 4.4 and 4.5

The table below lists the standard deviations of the flap blade root moment (Mb), nodding displacement of the tower (xnod), the tilt and yaw moment on the nacelle (Mtilt, Myaw) and the driving torque on the shaft (Mshaft) for the four options

	0p	0,1p	0,1,2p	0,1,2,3p
std Mb	6.3786e+005	5.4099e+005	5.1445e+005	5.0724e+005
std xnod	4.4374e-002	4.4172e-002	4.4613e-002	5.1612e-002
std Mtilt	5.6630e+005	4.4185e+005	3.4648e+005	3.4652e+005
std Myaw	5.3480e+005	3.9728e+005	3.4023e+005	3.4041e+005
std Mshaft	2.7660e+005	2.7665e+005	2.7662e+005	2.3964e+005

The 1p-mode suppression is responsible for the major part of potential mode-load reduction in the blade flap moment.

The 2p-mode suppression is responsible for the major part of potential mode-load reduction in the tilt and yaw moment.

Figure 4.6 shows the autopower spectra of the flapwise blade root moment and tiltwise moment on the nacelle in rotor centre; figure 4.7 shows those spectra of the yawwise moment and the rotor moment. Figures 4.8 and 4.9 show the relative fatigue load reduction in the flap moment and tilt moment as obtained from the three individual pitch control options. The slope values ‘m=10,11’ correspond to plastic materials while the values ‘m=3,4’ correspond to steel.

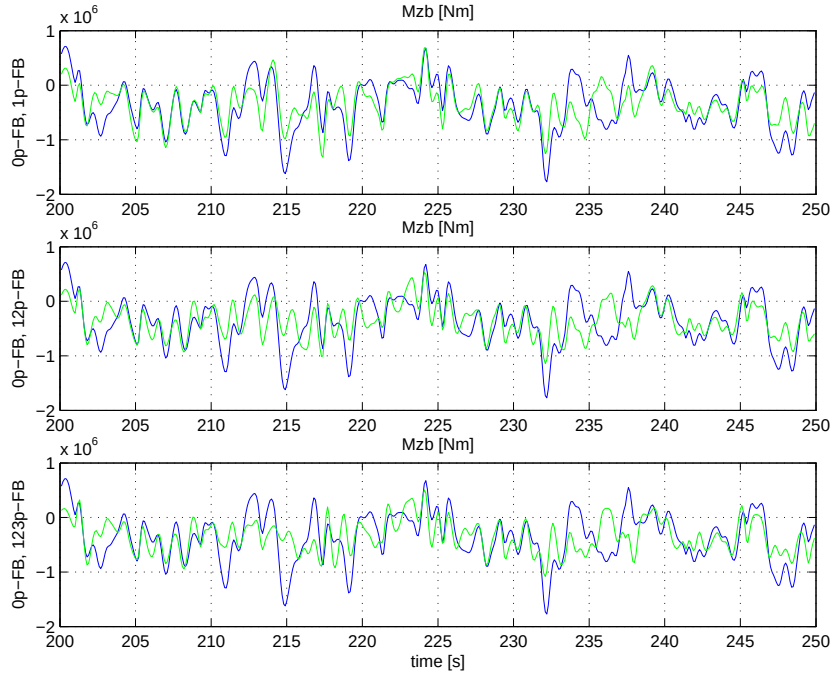

Figure 4.1: Realisations of flapwise blade root moment (dotted lines: individual pitch control included)

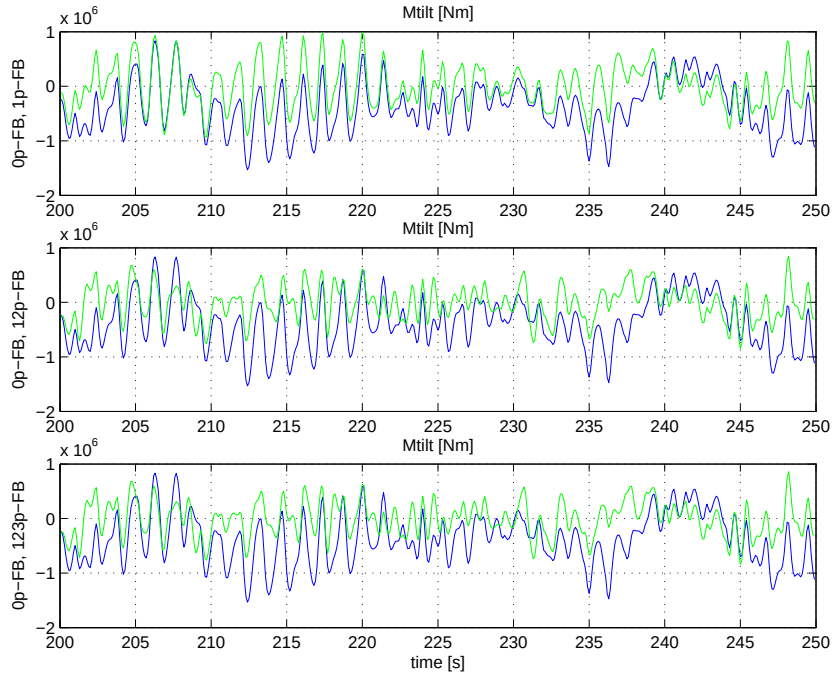

Figure 4.2: Realisations of tiltwise moment on nacelle in rotor centre (dotted lines: individual pitch control included)

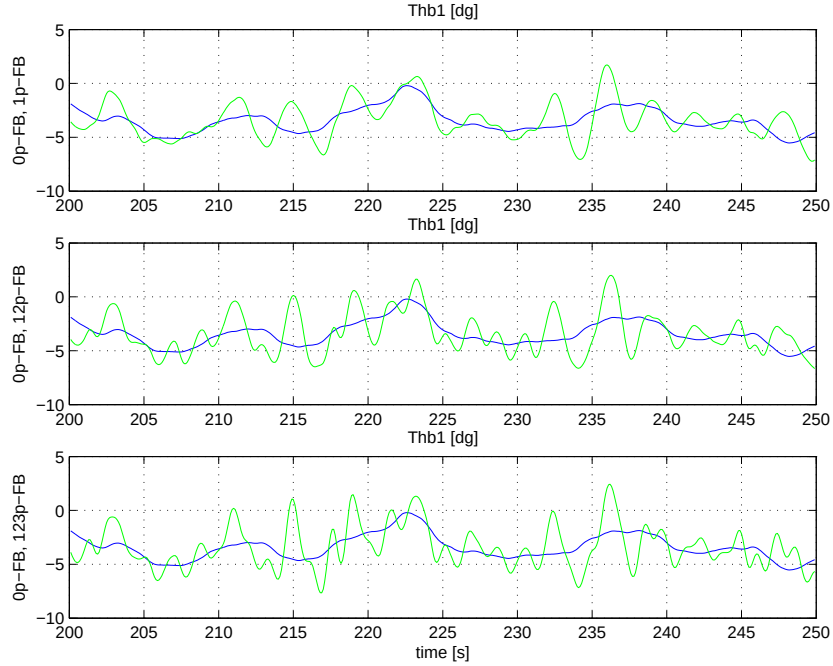

Figure 4.3: Realisations of pitch angle (dotted lines: individual pitch control included)

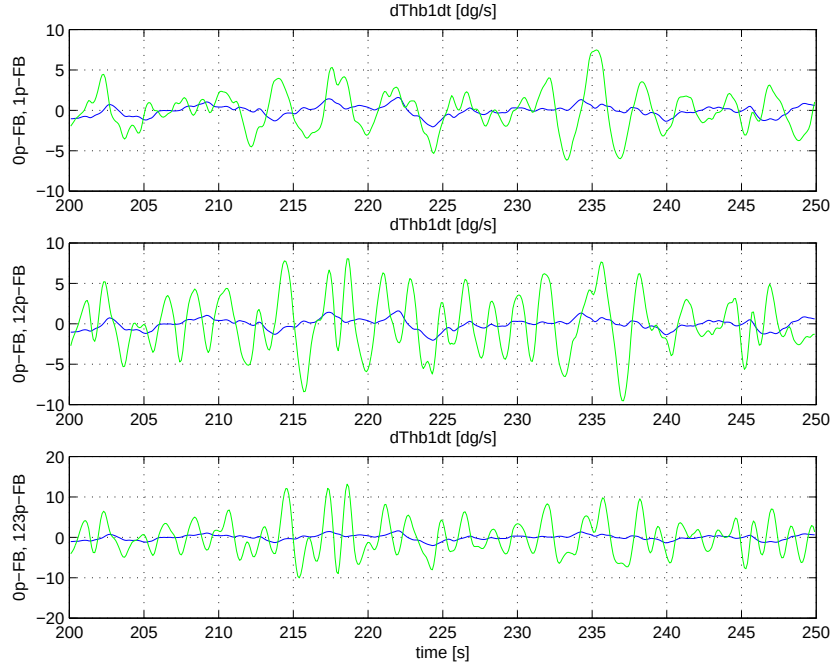

Figure 4.4: Realisations of pitch speed (dotted lines: individual pitch control included)

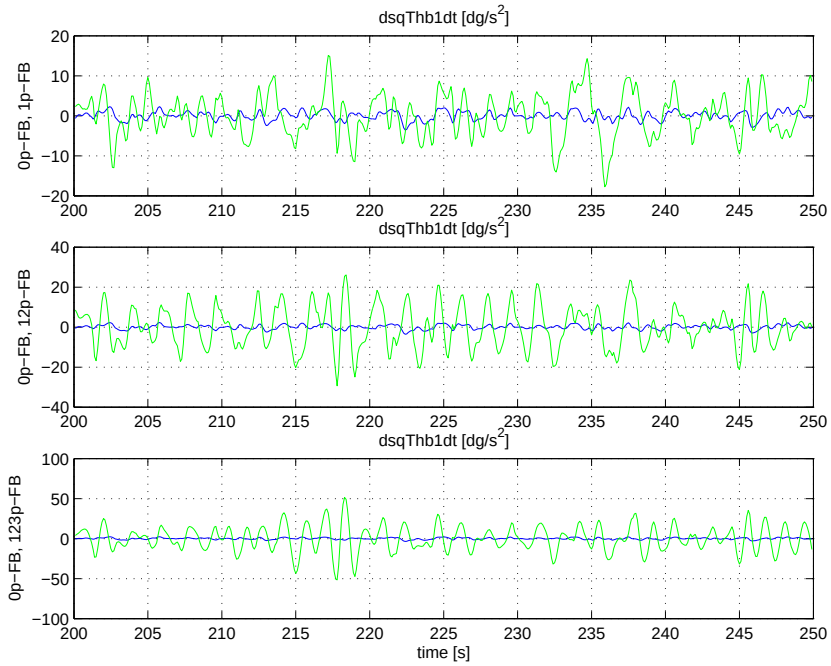

Figure 4.5: Realisations of pitch accelerations (dotted lines: individual pitch control included)

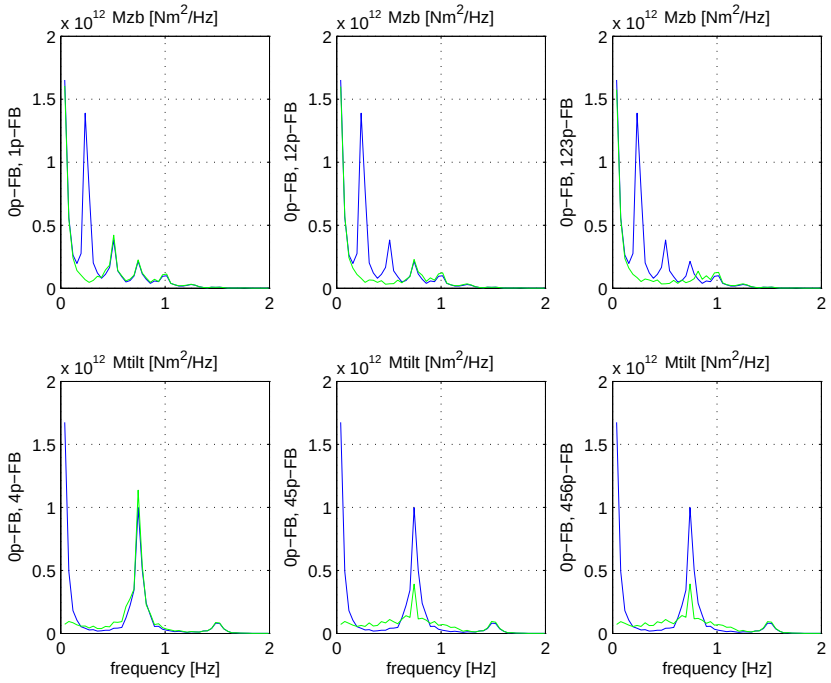

Figure 4.6: Autopower spectra of flapwise blade root moment and tiltwise moment in rotor centre (dotted lines: individual pitch control included)

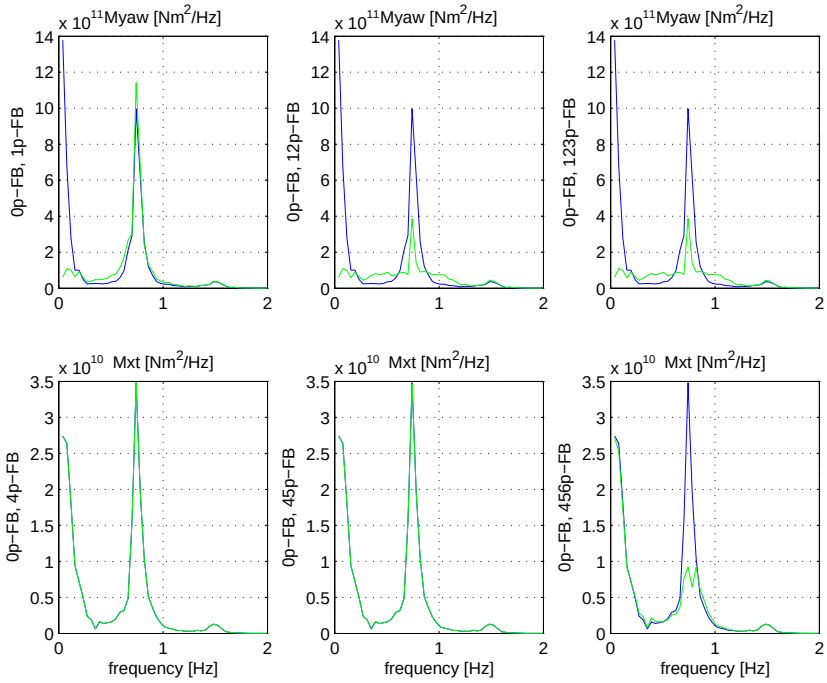

Figure 4.7: Autopower spectra of rotor moment and yawwise moment on nacelle in rotor centre (dotted lines: individual pitch control included)

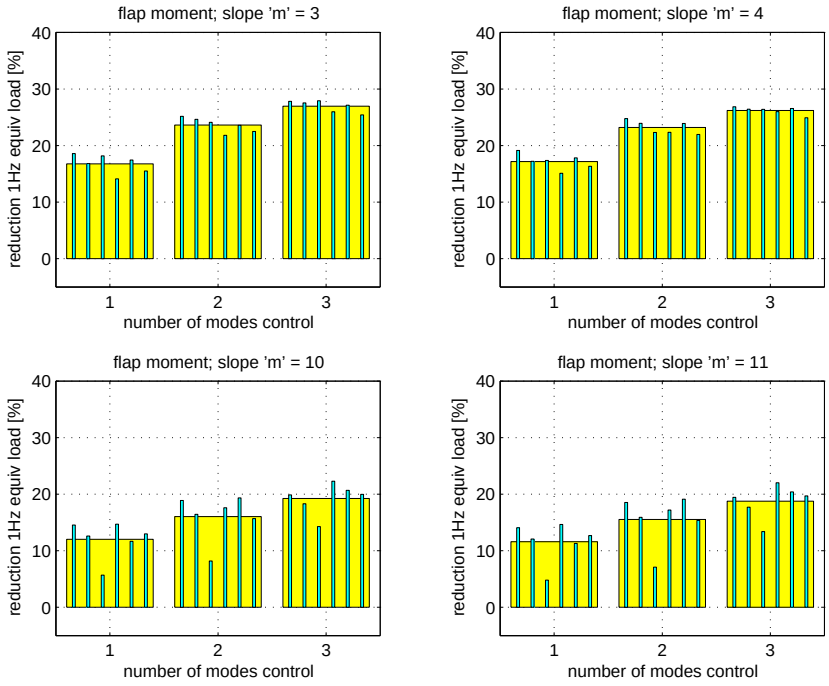

Figure 4.8: Relative fatigue load reduction in flapwise blade root moment on nacelle in rotor centre (narrow bars: realisations over 800s; wide bars: average over six realisations in 15 m/s)

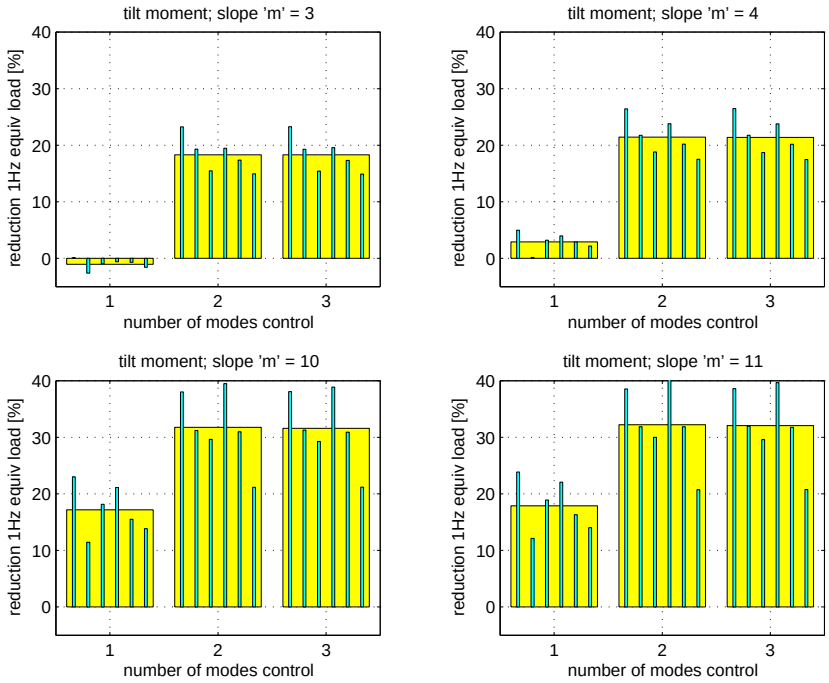

Figure 4.9: Relative fatigue load reduction in tiltwise moment on nacelle in rotor centre (narrow bars: realisations over 800s; wide bars: average over six realisations in 15 m/s)

5 CONCLUSION

A simple design model has been derived for the parametrisation of feedback loops for individual pitch control around one time the rotational frequency (1p) for 3 baded wind turbines. Stability assessment according to Bode can be applied to the three resulting independent control loops (phase and gain margins). The feedback approach to individual pitch control enables to reduce loads arising from tower shadow and wind shear as well as from turbulence.

Rainflow counts and power spectra obtained from time-domain simulations give an indication of the achievable reduction of loads. In addition, the concept of individual pitch control is extendend to multiples of the rotational frequency (2p, 3p; multi-rotational-mode pitch control). Scoping calculations show a significant further reduction of blade loads as well as a reduction of 3p harmonics in tilt and yaw loads in the nacelle. Fatigue load reduction up to 20 % in frequently occurring full load conditions seems realistic. Analytic stability assessment for multi-rotational-mode control has not yet been performed. This is a high-priortiy topic for further research.

REFERENCES

[1] E. Bossanyi. Individual blade pitch control for load reduction. In *Wind Energy, 119-128.* 2003.

[2] P. Caselitz, W. Kleinkauf, W. Krueger, J. Petschenka, M. Reichardt, and K. Stoerzel. Reduction of fatigue loads on wind energy converters by advanced control methods. In *Proc. European Wind Energy Conference, Dublin, 555-558*, Irish Wind Eenrgy Assoc. 1997.

[3] Coleman, R.P. and A.M. Feingold. "Theory of Self-Excited Mechanical Oscillations of Helicopter Rotors with Hinged Blades". NASA TN 3844, NASA, Februari 1957.

A GAINS FOR BLADE LOADS

The gains from pitch and wind speed variations (k..., h...) towards the aerodynamic loads per blade in rotor centre are all derived from power and thrust coefficient data.

```
%   kmx == dMxdTh =  1/3 * dTae/dTh
%   kmz == dMzdTh =       -dMflap/dTh
%   kfz == dFzdTh =        dFlead/dTh
%   kfx == dFxdTh =  1/3 * dFax/dTh
%   hmx == dMxdVw =  1/3 * dTae/dVw
%   hmz == dMzdVw =       -dMflap/dVw
%   hfz == dFzdVw =        dFlead/dVw
%   hfx == dFxdVw =  1/3 * dFax/dVw
%
%  Expressions for used sensitivities in calculated gains:
%
%   dTae/dTh = (Tae(Vw0,Th0+DTh,Omg0) - Tae(Vw0,Th0,Omg0))/DTh
%
%                NoAnn
%   dMflap/dTh = sum RsAnn(j)*{Fflap(j,Vw0,Th0+DTh,Omg0) - Fflap(j,Vw0,Th0,Omg0)}/DTh
%                j=1
%
%                NoAnn
%   dFlead/dTh = sum {Flead(j,Vw0,Th0+DTh,Omg0) - Flead(j,Vw0,Th0,Omg0)}/DTh
%                j=1
%
%   dFax/dTh = (Fax(Vw0,Th0+DTh,Omg0) - Fax(Vw0,Th0,Omg0))/DTh
%
%   dTae/dVw = (Tae(Vw0+DVw,Th0,Omg0) - Tae(Vw0,Th0,Omg0))/DVw
%
%                NoAnn
%   dMflap/dVw = sum RsAnn(j)*{Fflap(j,Vw0+DVw,Th0,Omg0) - Fflap(j,Vw0,Th0,Omg0)}/DVw
%                j=1
%
%                NoAnn
%   dFlead/dVw = sum {Flead(j,Vw0+DVw,Th0,Omg0) - Flead(j,Vw0,Th0,Omg0)}/DVw
%                j=1
%
%   dFax/dVw = (Fax(Vw0+DVw,Th0,Omg0) - Tae(Vw0,Th0,Omg0))/DVw
%
%  in which the lead and flapwise forces Flead(j) and Fflap(j) in the annuli are
%  calculated under the assumption of equal aerodynamic efficiency per annulus:
%
%                                                          NoAnn
%   => lead force equal in each annulus:    Flead(j)=1/3*(Tae / (sum(RsAnn(i))
%                                                          i=1
%
%                                                                NoAnn
%   => flap force prop. to annulus radius:  Fflap(j)=RsAnn(j)*1/3*Fax / (sum(RsAnn(i))
%                                                                i=1
%
% with
%  Fax(Vw0,Th0,Omg0)     = 0.5*rho*pi*Rb^2*Ct(Vw0,Th0,Omg0)*Vw0^2;
%  Tae(Vw0,Th0,Omg0)     = 0.5*rho*pi*Rb^2*Cp(Vw0,Th0,Omg0)*Vw0^3/Omg0;
%  Tae(Vw0+DVw,Th0,Omg0) = 0.5*rho*pi*Rb^2*Cp(Vw0+DVw,Th0,Omg0)*(Vw0+DVw)^3/Omg0;
%  Tae(Vw0,Th0+DTh,Omg0) = 0.5*rho*pi*Rb^2*Cp(Vw0,Th0+DTh,Omg0)*Vw0^3/Omg0;
%  Fax(Vw0+DVw,Th0,Omg0) = 0.5*rho*pi*Rb^2*Ct(Vw0+DVw,Th0,Omg0)*(Vw0+DVw)^2;
%  Fax(Vw0,Th0+DTh,Omg0) = 0.5*rho*pi*Rb^2*Ct(Vw0,Th0+DTh,Omg0)*Vw0^2;
```

```
%
% in which:
%  Cp(Vw0,Th0,Omg0)     = Cp(Th0,Omg0*Rb/Vw0);
%  Ct(Vw0,Th0,Omg0)     = Ct(Th0,Omg0*Rb/Vw0);
%  Cp(Vw0+DVw,Th0,Omg0) = Cp(Th0,Omg0*Rb/(Vw0+DVw))
%  Ct(Vw0+DVw,Th0,Omg0) = Ct(Th0,Omg0*Rb/(Vw0+DVw))
%  Cp(Vw0,Th0+DTh,Omg0) = Cp(Th0+DTh,Omg0*Rb/Vw0)
%  Ct(Vw0,Th0+DTh,Omg0) = Ct(Th0+DTh,Omg0*Rb/Vw0)
```

*

	Datum: June 2005	**Rapport No.:** ECN-C--03-138
Titel	Individual Pitch Control Inventory	
Auteur(s)	T.G. van Engelen, E.L. van der Hooft	
Opdrachtgever(s)	Novem, Dutch Ministry of Economic Affairs	
ECN projectnummer **Opdrachtgever ordernummer**	7.5153 2020-01-12-10-003	
Programma('s)	BSE, Doelsubsidie	

Abstract
The loads on the rotor blades, drive-train and tower of horizontal axis wind turbines are caused for a significant part by the rotational sampling of turbulence, the tower shadow and the windshear. These loads depend on the azimutal blade position and are approximately periodic in (multiples of) the rotational speed. It seems attractive to just add pure azimut dependent variations to the pitch angle of the individual blades. However, a small phase mismatch with respect to the tower shadow and windshear effect will cause higher instead of lower loads. Besides, the stochastic loads from the rotationally sampled turbulence are not reduced at all.

This inventory study concerns the design and potential of individual *feedback* pitch control for 3 bladed wind turbines. In this approach the danger of mismatch is avoided and the stochastic blade loads are also reduced. A simple design model is derived for the parametrisation of the feedback loops for individual pitch control around one time the rotational frequency (1p). Rainflow counts and power spectra obtained from time-domain simulations give an indication of the achievable reduction of loads. In addition, the concept of individual pitch control is extendend to multiples of the rotational frequency (2p, 3p; multi-mode pitch control). Scoping calculations show a significant further reduction of blade loads as well as a reduction of 3p harmonics in tilt and yaw loads in the nacelle.

Keywords
windturbine, individual pitch control, blade loads, yaw bearing loads

Authorisatie	**Naam**	**Handtekening**	**Datum**
Gecontroleerd			
Goedgekeurd			
Geauthoriseerd			